

BRIDGE TO REAL DATA: EMPIRICAL MULTIPLE MATERIAL CALIBRATION FOR LEARNING-BASED MATERIAL DECOMPOSITION

Yanye Lu^{1,2,4}, Martin Berger¹, Michael Manhart^{1,2}, Jang-hwan Choi³, Martin Hoheisel², Markus Kowarschik², Rebecca Fahrig^{2,3}, Qiushi Ren⁴, Joachim Hornegger¹, Andreas Maier¹

¹Pattern Recognition Lab, Department of Computer Science,
Friedrich-Alexander-University Erlangen-Nuremberg, Germany
²Advanced Therapies, Siemens Healthcare GmbH, Forchheim, Germany
³Radiological Sciences Lab, Stanford University, CA, USA
⁴Department of Biomedical Engineering,
Peking University, Beijing, China

ABSTRACT

In this study, we proposed an empirical multi-material calibration pipeline for learning-based material decomposition. We used realistic short scan CT data from a general metric phantom using a Siemens C-arm system, and built the corresponding numeric phantom data in a software framework. After that we applied registration approaches for matching the simulated data to the acquired data, which generates prior knowledge for the following material decomposition process, as well as the ground truth for quantitative evaluations. According to the preliminary decomposition results, we successfully decomposed the inserted phantom plugs of different materials using learning-based material decomposition process, which indicates that the proposed approach is valid for learning-based material decomposition.

1. INTRODUCTION

Spectral computed tomography (CT) started around 1975 as an improvement in CT technology, which enables to gain information on the energy-dependent attenuation properties of the object [1]. This makes it possible to differentiate different base materials in X-ray imaging, as long as the number of detector bins is equal or greater than the number of basis materials. The first algorithm is called the “basis material decomposition” (BMD) method [2], and was proposed in 1976. The BMD method has been applied to many clinical and scientific applications for material decomposition. Since most material decomposition methods are extended from the BMD method, spectral weighting or spectrum calibration are essential for these methods [3][4][5]. However, it is difficult to measure polychromatic spectral information in realistic scans, which limits the accuracy of material decomposition. To avoid these difficulties, empirical calibration techniques that use measurements of known materials with known positioning are employed to analytically derive the correlations of the materials and the path length [6]. In order to bring

those approaches closer to clinical applications, we applied an empirical multi-material calibration for a learning-based material decomposition process. We performed several experiments to investigate the feasibility of the calibration. The results are evaluated using linear correlation (r) and the structural similarity index (SSIM) [7] as quantitative metrics.

2. METHODS

In this study, we used short scan CT data from CRIS’s Electron Density Phantom Model 062 (CIRS, Norfolk, Virginia, USA) using a Siemens C-arm CT system. Additionally we built the corresponding numeric phantom data in a software framework. After that we applied registration approaches for matching the simulated data to the acquired data, which generates not only prior knowledge but also ground truth for the following material decomposition process, as well as the ground truth for quantitative evaluations. All methods are implemented in Java-based framework CONRAD [8].

2.1. Data Generation

The CRIS’s Electron Density Phantom Model 062 (ED phantom) is specifically designed for Cone Beam CT Imaging systems, which enables precise correlation of CT data to electron density of various tissues. It consists of two nested disks made from material of water equivalent plastic. They can represent both head and abdomen configurations. We only used the inner disk in this study, in which 9 different tissue equivalent electron density inserted phantom plugs can be positioned within the scan field. Optional distance marker plugs enable quick assessment of the CT scanner’s distance measurement accuracy. The configuration of the ED phantom is presented in Figure 1.

For the real data, we performed scans of the ED phantom at three different tube voltage settings of 50kV, 90kV and 125kV. During these scans, the maximal axial collima-

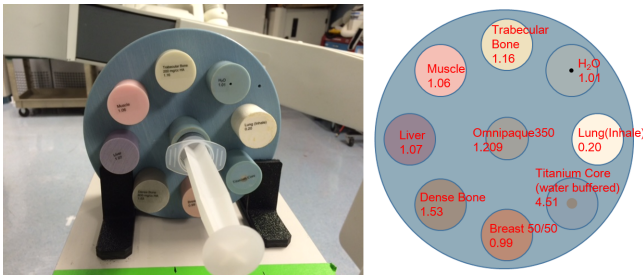


Fig. 1. The CRIS's Electron Density Phantom Model 062 and the corresponding analytic description.

tion was used to reduce scatter artifacts. The resolution of the flat panel detector is 2480x1920 pixels with a pixel size of 0.154x0.154 mm, however in this study the detector was operated with 2x2 binning that allows an effective resolution of 1240x1920 pixels with a pixel size of 0.308x0.308 mm. The source-to-isocenter distance is 600 mm while the source-to-detector distance is 1200 mm. Rotation of 197.53 degrees short scans with an average angular increment of 0.76 per projection were performed, which generated 248 projections for each scan.

The numeric ED phantom data generation relies on the simulation of X-ray images [9]. We used the analytic description of the ED phantom, as well as the same scanning setups of the realistic CT scan, to build the corresponding numeric phantom data. For the X-ray spectrum setup, we applied the effective monochromatic X-ray energy dependent absorption model to the data. Energy-dependent X-ray absorption coefficients for elemental data and compounds were obtained from the NIST database [10].

2.2. Data Calibration

The C-arm scanner generates absorption images, therefore we extracted line integrals using a Siemens software with the machine-dependent pre-processing. Then reconstruction was performed to yield 3-dimensional (3D) volume data of the ED phantom, additionally we applied a circular mask to limit the region-of-interest for the subsequent registration. On the other side, we built the numeric ED phantom data in 3D using the volumetric phantom renderer in CONRAD, as well as the individual materials data. Then we applied 3D-3D rigid registration [11] between the actual data and simulated ED phantom data to obtain the registration transform. For the rigid registration, the fixed image is the acquired data and the moving image the numeric ED phantom data.

Since the simulated ED phantom data and the individual materials in the ED phantom data have the same geometry, we registered the individual ED phantom data to the acquired data using the registration transform that comes from the 3D-3D registration. Finally we performed forward projection to the individual materials in the ED phantom data to yield the

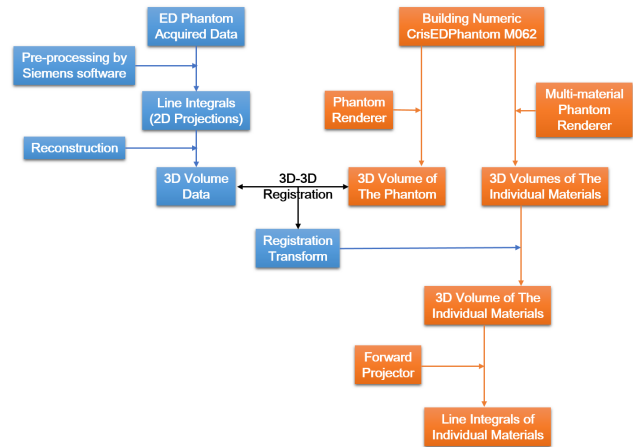


Fig. 2. The calibration procedure flow chart

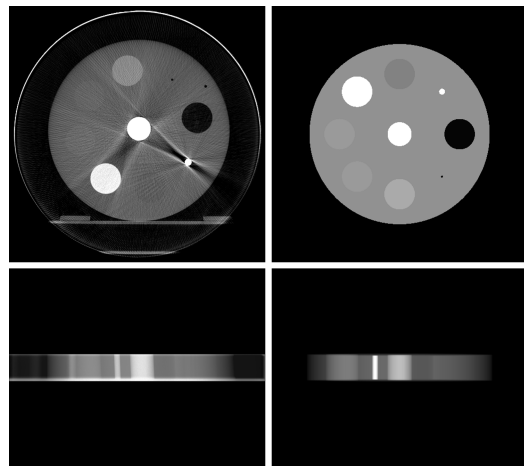


Fig. 3. Two examples of the acquired ED Phantom data (left) and the simulated multiple materials ED phantom data (right) at the tube voltage of 90kV.

individual materials projection data for material decomposition [12] in projection domain, as well as the ground truth for the quantitative evaluation of linear correlation and the SSIM index. The calibration procedure flow chart is illustrated in Figure 2.

2.3. Learning-based Material Decomposition

Firstly, we extracted 5 consecutive frames as a subset of the acquired data, and used the first frame from the acquired data and the simulated phantom data respectively for classifier training, then we employed learning-based material decomposition approaches to predict the following frames (the second frame to the fifth frame). We performed the machine learning approaches of Bootstrap Aggregating (Bagging) using REPTrees for the material decomposition. We built feature extractors to extract the spectral information

(namely “Channel”) [3] and polynomial combinations [4] of the spectral information (namely “Polynomial”), and the Trainable Weka segmentation (namely “WEKA”) [13] that extracted structural information from the individual material ED phantom data, from both label images and training images for building the classifier by the machine learning approach of Bootstrap Aggregating (Bagging) with the WEKA implementation [14]. Additionally, following the above strategy, we applied the learning-based material decomposition process to all acquired projection images. We chose one frame of every 5 frames of the datasets as label data, which means there is an interval of 4 frames between two label frames. These label frames were used for supervised machine learning to build the classifiers, then we used the classifiers to predict the rest of the frames for the material decomposition process. Therefore, for the 248-frame dataset, we learned from 49 frames and predicted 199 frames. More details of the learning-based material decomposition method were elaborated in [12].

3. RESULTS

Figure 3 shows examples of the acquired ED phantom data, the simulated multi-material ED phantom data in 3D volume at a tube voltage of 80 kV. Since we knew the analytic description of the ED phantom, we could easily see the misalignment. Figure 4 illustrates the 3D-3D registration procedure. After the registration, the misalignment is eliminated. Now the individual material phantom data in projection domain could be used as the label images for the learning-based material decomposition process, as well as the ground truth for the quantitative evaluation. Figure 5 and Figure 6 show the material decomposition results of titanium rod, dense bone and water, and the respective reconstructions of the material decomposition results, along with the quantitative results.

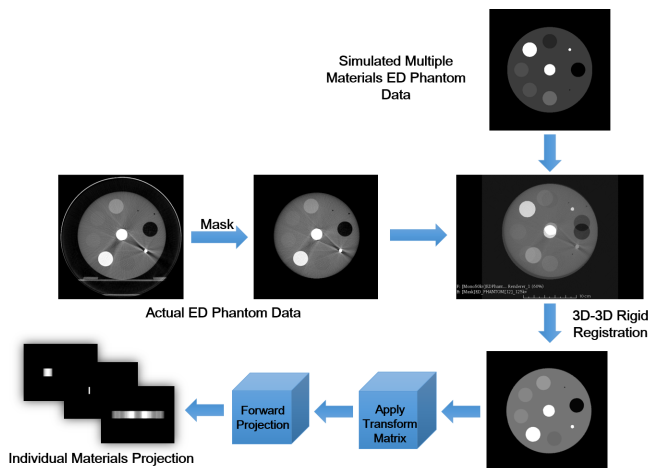


Fig. 4. The 3D-3D registration procedure

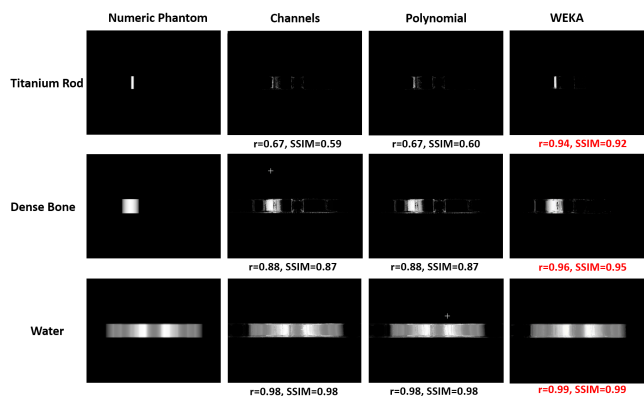


Fig. 5. The material decomposition results of titanium rod, dense bone and water, as well as the quantitative evaluation results.

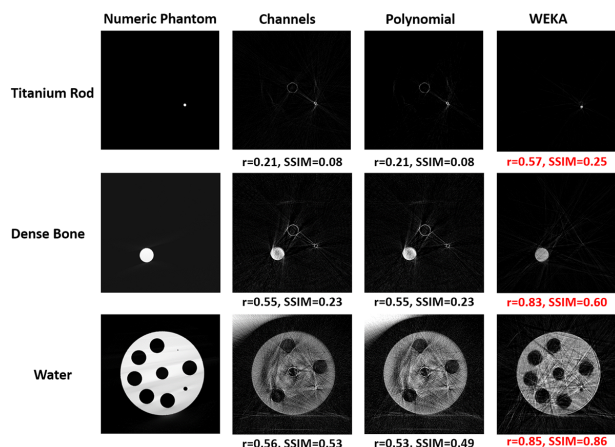


Fig. 6. Central slice of the material decomposition reconstruction, and the quantitative evaluation results.

4. DISCUSSION AND CONCLUSION

In this study, we proved the concept of calibrating multi-material phantom using a registration method. We built the corresponding numeric phantom data using the analytic description of the phantom and the actual scanning setup information. This yielded the registered individual multi-material phantom data for the learning-based material decomposition process, as well as the ground truth for the quantitative evaluation. We presented the results of the third frame to demonstrate the feasibility of the proposed approach. As shown in Figure 5, the utilization of energy-selective channels and their polynomial combination as features provide good results in distinguishing individual materials from the actual CT data, which is in line with our expectation. Furthermore, the decomposition results of using structural information (WEKA column in Figure 5 and Figure 6) are very good, which can be comparable or even better than results using other features.

Especially in the water reconstructed results (Figure 6), the “Channel” and the “Polynomial” results failed to distinguish the boundaries between water and the inserts that have similar attenuation coefficients compared to water. However, the “WEKA” result could differentiate the boundaries by benefiting from the shape information from the WEKA trainable segmentation features, which indicates the potential of integrating structural information into material decomposition. According to the preliminary decomposition results, we successfully decomposed the plugs of different materials using learning-based material decomposition process, which indicates that the empirical multiple materials calibration is valid for learning-based material decomposition.

5. ACKNOWLEDGMENT

The authors gratefully acknowledge funding support from the NIH Shared Instrument Grant S10 RR026714 supporting the zeego@StanfordLab, and Siemens AT. The authors also gratefully acknowledge funding of the Research Training Group 1773 Heterogeneous Image Systems and the Erlangen Graduate School in Advanced Optical Technologies (SAOT) by the German Research Foundation (DFG).

Disclaimer: The concepts and information presented in this paper are based on research and are not commercially available.

6. REFERENCES

- [1] B. Heismann, B. Schmidt, and T. Flohr, *Spectral Computed Tomography*. SPIE, 2012.
- [2] R. E. Alvarez and A. Macovski, “Energy-selective reconstructions in x-ray computerised tomography,” *Physics in Medicine and Biology*, vol. 21, no. 5, p. 733, 1976.
- [3] M. Firsching, P. Takoukam Talla, T. Michel, and G. Anton, “Material resolving x-ray imaging using spectrum reconstruction with medipix2,” *Nuclear Instruments and Methods in Physics Research Section A: Accelerators, Spectrometers, Detectors and Associated Equipment*, vol. 591, no. 1, pp. 19–23, 2008.
- [4] N. Maass, S. Sawall, M. Knaup, and M. Kachelriess, “Empirical multiple energy calibration (emec) for material-selective ct,” in *Nuclear Science Symposium and Medical Imaging Conference (NSS/MIC), 2011 IEEE*, pp. 4222–4229, Oct 2011.
- [5] C. Maass, E. Meyer, and M. Kachelriess, “Exact dual energy material decomposition from inconsistent rays (mdir),” *Medical Physics*, vol. 38, no. 2, pp. 691–700, 2011.
- [6] P. Stenner, T. Berkus, and M. Kachelriess, “Empirical dual energy calibration (edec) for cone-beam computed tomography,” *Medical Physics*, vol. 34, no. 9, pp. 3630–3641, 2007.
- [7] Z. Wang, A. Bovik, H. Sheikh, and E. Simoncelli, “Image quality assessment: from error visibility to structural similarity,” *Image Processing, IEEE Transactions on*, vol. 13, pp. 600–612, April 2004.
- [8] A. Maier, H. G. Hofmann, M. Berger, P. Fischer, C. Schwemmer, H. Wu, K. Müller, J. Hornegger, J.-H. Choi, C. Riess, A. Keil, and R. Fahrig, “Conrad-a software framework for cone-beam imaging in radiology,” *Medical Physics*, vol. 40, no. 11, p. 111914, 2013.
- [9] A. Maier, H. G. Hofmann, C. Schwemmer, J. Hornegger, A. Keil, and R. Fahrig, “Fast simulation of x-ray projections of spline-based surfaces using an append buffer,” *Physics in Medicine and Biology*, vol. 57, no. 19, p. 6193, 2012.
- [10] J. H. Hubbell and S. M. Seltzer, “Tables of X-ray mass attenuation coefficients and mass energy-absorption coefficients,” tech. rep., National Inst. of Standards and Technology-PL, Gaithersburg, MD (United States). Ionizing Radiation Div., 1995.
- [11] A. Collignon, F. Maes, D. Delaere, D. Vandermeulen, P. Suetens, and G. Marchal, “Automated multi-modality image registration based on information theory,” in *Information Processing in Medical Imaging*, 1995.
- [12] Y. Lu, J. Geret, M. Unberath, M. Manhart, Q. Ren, R. Fahrig, J. Hornegger, and A. Maier, “Projection-based material decomposition by machine learning using image-based features for computed tomography,” in *The 13th International Meeting on Fully Three-Dimensional Image Reconstruction in Radiology and Nuclear Medicine*, pp. 448–451, June 2015.
- [13] I. Arganda-Carreras, A. Cardona, V. Kaynig, and J. Schindelin, “Trainable weka segmentation,” *Fiji website*, 2013.
- [14] E. Hall, Mark and Frank, G. Holmes, B. Pfahringer, P. Reutemann, and I. H. Witten, “The WEKA data mining software: An update,” *SIGKDD Explorations*, vol. 11, no. 1, pp. 10–18, 2009.